Methane-to-Methanol Conversion by First-Row Transition-Metal Oxide Ions: ScO^+, TiO^+, VO^+, CrO^+, MnO^+, FeO^+, CoO^+, NiO^+, and CuO^+

Yoshihito Shiota and Kazunari Yoshizawa*

Contribution from the Department of Molecular Engineering, Kyoto University, Sakyo-ku, Kyoto 606-8501, Japan

Received May 23, 2000. Revised Manuscript Received September 15, 2000

Abstract: The reaction pathway and energetics for methane-to-methanol conversion by first-row transition-metal oxide ions (MO^+s) are discussed from density functional theory (DFT) B3LYP calculations, where M is Sc, Ti, V, Cr, Mn, Fe, Co, Ni, and Cu. The methane-to-methanol conversion by these MO^+ complexes is proposed to proceed in a two-step manner via two transition states: $MO^+ + CH_4 \rightarrow OM^+(CH_4) \rightarrow [TS] \rightarrow OH-M^+-CH_3 \rightarrow [TS] \rightarrow M^+(CH_3OH) \rightarrow M^+ + CH_3OH$. Both high-spin and low-spin potential energy surfaces are characterized in detail. A crossing between the high-spin and the low-spin potential energy surfaces occurs once near the exit channel for ScO^+, TiO^+, VO^+, CrO^+, and MnO^+, but it occurs twice in the entrance and exit channels for FeO^+, CoO^+, and NiO^+. Our calculations strongly suggest that spin inversion can occur near a crossing region of potential energy surfaces and that it can play a significant role in decreasing the barrier heights of these transition states. The reaction pathway from methane to methanol is uphill in energy on the early MO^+ complexes (ScO^+, TiO^+, and VO^+); thus, these complexes are not good mediators for the formation of methanol. On the other hand, the late MO^+ complexes (FeO^+, NiO^+, and CuO^+) are expected from the general energy profiles of the reaction pathways to efficiently convert methane to methanol. Measured reaction efficiencies and methanol branching ratios for MnO^+, FeO^+, CoO^+, and NiO^+ are rationalized from the energetics of the high-spin and the low-spin potential energy surfaces. The energy diagram for the methane-to-methanol conversion by CuO^+ is downhill toward the product direction, and thus CuO^+ is likely to be an excellent mediator for methane hydroxylation.

Introduction

The development of catalysts for selective oxidation of saturated hydrocarbons under mild conditions is a central research subject in modern chemistry.[1−7] Studies on the gas-phase reactions of bare transition-metal ions and hydrocarbons have provided a wealth of insight concerning the intrinsic interactions between the active site of catalysts and organic substrates.[8−11] The direct conversion of methane to methanol is thermodynamically favorable compared to the commercial two-step process via synthesis gas (CO and H_2),[12] and therefore it is of current interest in pure and applied chemistry. The catalytic activity of bare transition-metal monoxide cations (MO^+) toward methane is a key to the mechanistic aspects in the direct methane hydroxylation.[13−15] Schröder, Schwarz, and co-workers have systematically investigated the gas-phase reactions of the first-row MO^+ complexes and methane,[14,16] demonstrating that late MO^+ complexes are able to activate methane. The reaction efficiency and the methanol branching ratio are significantly dependent on the metals. For example, FeO^+ efficiently reacts with methane under ion cyclotron resonance (ICR) conditions, forming methanol in 41% yield.[14a] Although MnO^+ reacts with methane very efficiently, the branching ratio to methanol is less than 1%.[14d] CoO^+ exhibits low reactivity toward methane, but the branching ratio to methanol is 100%.[15b] Both the reactivity and the methanol

* To whom correspondence should be addressed. E-mail: kazunari@scl.kyoto-u.ac.jp.

(1) (a) Shilov, A. E. *The Activation of Saturated Hydrocarbons by Transitions Metal Complexes*; Riedel Publishing: Dordrecht, The Netherlands, 1984. (b) Shilov, A. E.; Shul'pin, G. B. *Chem. Rev.* **1997**, *97*, 2879. (c) Shilov, A. E.; Shteinman, A. A. *Acc. Chem. Res.* **1999**, *32*, 763.

(2) Hill, C. L., Ed. *Activation and Functionalization of Alkanes*; Wiley: New York, 1989.

(3) Davies, J. A.; Watson, P. L.; Liebman, J. F.; Greenberg, A. *Selective Hydrocarbon Activation*; VCH: New York, 1990.

(4) (a) Crabtree, R. H. *The Organometallic Chemistry of the Transition Metals*; Wiley: New York, 1990. (b) Crabtree, R. H. *Chem. Rev.* **1985**, *85*, 245. (c) Crabtree, R. H. *Chem. Rev.* **1995**, *95*, 987.

(5) Arndtsen, B. A.; Bergman, R. G.; Mobley, T. A.; Peterson, T. H. *Acc. Chem. Res.* **1995**, *28*, 154.

(6) Hall, C.; Perutz, R. N. *Chem. Rev.* **1996**, *96*, 3125.

(7) Lunsford, J. H. *Angew. Chem., Int. Ed. Engl.* **1995**, *34*, 970.

(8) Armentrout, P. B. *Science* **1991**, *251*, 175.

(9) Eller, K.; Schwarz, H. *Chem. Rev.* **1991**, *91*, 1121.

(10) Roth, L. M.; Freiser, B. S. *Mass Spectrom. Rev.* **1991**, *10*, 303.

(11) Weisshaar, J. C. *Acc. Chem. Res.* **1993**, *26*, 213.

(12) Gesser, H. D.; Hunter, N. R.; Prakash, C. B. *Chem. Rev.* **1985**, *85*, 235.

(13) (a) Jackson, T. C.; Jacobson, D. B.; Freiser, B. S. *J. Am. Chem. Soc.* **1984**, *106*, 1252. (b) Kang, H.; Beauchamp, J. L. *J. Am. Chem. Soc.* **1986**, *108*, 5663. (c) Kang, H.; Beauchamp, J. L. *J. Am. Chem. Soc.* **1986**, *108*, 7502. (d) Jackson, T. C.; Carlin, T. J.; Freiser, B. S. *J. Am. Chem. Soc.* **1986**, *108*, 1120.

(14) (a) Schröder, D.; Schwarz, H. *Angew. Chem., Int. Ed. Engl.* **1990**, *29*, 1433. (b) Schröder, D.; Fiedler, A.; Hrusák, J.; Schwarz, H. *J. Am. Chem. Soc.* **1992**, *114*, 1215. (c) Ryan, M. F.; Fiedler, A.; Schröder, D.; Schwarz, H. *Organometallics* **1994**, *13*, 4072. (d) Ryan, M. F.; Fiedler, A.; Schröder, D.; Schwarz, H. *J. Am. Chem. Soc.* **1995**, *117*, 2033. (e) Schwarz, J.; Wesendrup, R.; Schröder, D.; Schwarz, H. *Chem. Ber.* **1996**, *129*, 1463.

(15) (a) Clemmer, D. E.; Aristov, N.; Armentrout, P. B. *J. Phys. Chem.* **1993**, *97*, 544. (b) Chen, Y.-M.; Clemmer, D. E.; Armentrout, P. B. *J. Am. Chem. Soc.* **1994**, *116*, 7815.

(16) A review: Schröder, D.; Schwarz, H. *Angew. Chem., Int. Ed. Engl.* **1995**, *34*, 1973.

10.1021/ja0017965 CCC: $19.00
Published on Web 11/21/2000

branching ratio are high in NiO^+.[16] In contrast, the early MO^+ complexes (ScO^+, TiO^+, and VO^+) exhibit no reactivity toward alkanes and alkenes, due to their strong metal−oxo bonds. Interestingly, Sc^+ reacts with methanol to yield ScO^+ and methane in the gas phase,[17] which is precisely the reverse reaction of methane hydroxylation.

From density functional theory (DFT) computations, we determined the reaction pathway and its detailed energetics for the direct methane−methanol conversion by FeO^+.[18] Two transition states (TS1 and TS2) were confirmed from intrinsic reaction coordinate[18d] and femtosecond dynamics[18e] calculations to correctly connect the reaction pathway indicated in eq 1. We have extended this study to other late MO^+ complexes and different charge states, MnO^+, CoO^+, FeO, and FeO^{2+}.[18b,c] Of course, this mechanism is not limited to the gas-phase methane hydroxylation by the bare MO^+ complexes. The direct benzene−phenol conversion by FeO^+ in the gas phase[19] and by an iron−oxo species over Fe−ZSM-5 zeolite[20] should take place in a similar manner. Moreover, we have extended this concerted mechanism to the methane hydroxylation by intermediate **Q** of soluble methane monooxygenase (sMMO),[21] in which a dinuclear iron−oxo complex plays an essential role as an active site. The question as to the reaction pathway and energetics for the methane-to-methanol conversion by the first-row MO^+ complexes and its answer are of particular interest in this article.

$$FeO^+ + CH_4 \rightarrow OFe^+(CH_4) \rightarrow [TS1] \rightarrow OH-Fe^+-CH_3 \rightarrow [TS2] \rightarrow Fe^+(CH_3OH) \rightarrow Fe^+ + CH_3OH \quad (1)$$

Another topic of interest in the methane-to-methanol conversion by metal−oxo species is the electronic process of spin inversion, which can occur in the vicinity of a crossing region of two potential energy surfaces of different spin states.[22] In contrast to organic reactions, which in most cases proceed on a single potential energy surface, reactions mediated by organometallic systems can proceed on more than one potential energy surface. For example, the reactions of FeO^+ with dihydrogen[22b,c] and methane[18b,e] have been analyzed in terms of the corresponding potential energy surfaces. It turned out that, besides the classical factors such as the potential barrier heights, the spin−orbit coupling factor is important because a crossing between the high-spin and the low-spin states constitutes a distinct mechanistic step along the reaction coordinate. This phenomenon called "two-state reactivity" is likely to be a key feature in organometallic chemistry.[22d]

A large amount of work has been performed on the oxidation of hydrocarbons on the surface of transition-metal oxides.[23−25] Anderson et al. carried out a systematic study of methane oxidation using a number of metal oxide catalysts, demonstrating that Co_3O_4 is the most active single-component catalyst.[23] Henrich and Cox compiled a list of studies of organic molecules on single-crystal transition-metal oxides.[24] The ease of reduction of M^{3+} ions, i.e., oxidation of organic substrates, follows the sequence:

$$Ti^{3+} < V^{3+} < Fe^{3+} < Mn^{3+} < Co^{3+} < Ni^{3+} \quad (2)$$

Thus, the oxidizing power rises with increasing atomic number in general. In this paper, we report the mechanism and energetics for the reactions between the MO^+ complexes of the first-row transition metals (from ScO^+ to CuO^+) and methane. Our discussions and conclusions are reasonably derived from DFT computations on the potential energy surfaces along the reaction pathway. The FeO^+ complex has been extensively investigated with respect to its reactivity toward dihydrogen and methane, but our knowledge of the other MO^+ complexes is still limited in terms of energetics for the catalytic function. We systematically look at the methane hydroxylation by the first-row MO^+ complexes.

Method of Calculation

Computations were carried out with the Gaussian 94 ab initio program package.[26] The energies and geometries of the reactants, intermediates, products, and transition states were calculated with Becke's three-parameter hybrid functional[27] combined with the Lee, Yang, and Parr (LYP) correlation functional, denoted as B3LYP. The B3LYP energy expression is in the form of eq 3:

$$E_{XC}^{B3LYP} = (1 - a_0)E_X^{LSDA} + a_0E_X^{HF} + a_xE_X^{B88} + a_cE_C^{LYP} + (1 - a_c)E_C^{VWN} \quad (3)$$

$$a_0 = 0.20,\ a_x = 0.72,\ a_c = 0.81$$

in which E_X^{HF} is the Hartree−Fock exchange energy, E_X^{LSDA} is the local exchange energy from the local spin density approximation (LSDA), E_X^{B88} is Becke's gradient correction to the exchange functional, E_C^{LYP} is the correlation functional developed by Lee, Yang, and Parr,[28] and E_C^{VWN} is the correlation energy calculated using the local correlation functional of Vosko, Wilk, and Nusair (VWN).[29] The triple-ζ 6-311G** basis set of Pople and co-workers[30] was used for the carbon, oxygen, and hydrogen atoms, and the (14s9p5d) primitive set of Wachters[31] supplemented with one polarization f-function (α = 0.60 for Sc, 0.69 for Ti, 0.78 for V, 0.87 for Cr, 0.96 for Mn, 1.05 for Fe, 1.17 for Co,

(17) Azzaro, M.; Breton, S.; Decouzon, M.; Geribaldi, S. *Int. J. Mass Spectrom. Ion Processes* **1993**, *128*, 1.
(18) (a) Yoshizawa, K.; Shiota, Y.; Yamabe, T. *Chem. Eur. J.* **1997**, *3*, 1160. (b) Yoshizawa, K.; Shiota, Y.; Yamabe, T. *J. Am. Chem. Soc.* **1998**, *120*, 564. (c) Yoshizawa, K.; Shiota, Y.; Yamabe, T. *Organometallics* **1998**, *17*, 2825. (d) Yoshizawa, K.; Shiota, Y.; Yamabe, T. *J. Chem. Phys.* **1999**, *111*, 538. (e) Yoshizawa, K.; Shiota, Y.; Kagawa, Y.; Yamabe, T. *J. Phys. Chem. A* **2000**, *104*, 2552.
(19) Yoshizawa, K.; Shiota, Y.; Yamabe, T. *J. Am. Chem. Soc.* **1999**, *121*, 147.
(20) (a) Yoshizawa, K.; Yumura, T.; Shiota, Y.; Yamabe, T. *Bull. Chem. Soc. Jpn.* **2000**, *73*, 29. (b) Yoshizawa, K.; Shiota, Y.; Yumura, T.; Yamabe, T. *J. Phys. Chem. B* **2000**, *104*, 734.
(21) (a) Yoshizawa, K. *J. Biol. Inorg. Chem.* **1998**, *3*, 318. (b) Yoshizawa, K. *J. Inorg. Biochem.* **2000**, *78*, 23. (c) Yoshizawa, K.; Ohta, T.; Yamabe, T. *Bull. Chem. Soc. Jpn.* **1998**, *71*, 1899. (d) Yoshizawa, K.; Suzuki, A.; Shiota, Y.; Yamabe, T. *Bull. Chem. Soc. Jpn.* **2000**, *73*, 815.
(22) (a) Shaik, S.; Danovich, D.; Fiedler, A.; Schröder, D.; Schwarz, H. *Helv. Chim Acta* **1995**, *78*, 1393. (b) Danovich, D.; Shaik, S. *J. Am. Chem. Soc.* **1997**, *119*, 1773. (c) Filatov, M.; Shaik, S. *J. Phys. Chem. A* **1998**, *102*, 3835. (d) Schröder, D.; Shaik, S.; Schwarz, H. *Acc. Chem. Res.* **2000**, *33*, 139.
(23) Henrich, V. E.; Cox, P. A. *The Surface of Metal Oxides*; Cambridge University Press: Cambridge, 1994.
(24) Anderson, R. B.; Stein, K. C.; Feenan, J. J.; Hofer, L. J. E. *Ind. Eng. Chem.* **1961**, *53*, 809.
(25) Barteau, M. A. *Chem. Rev.* **1996**, *96*, 1413.
(26) Frisch, M. J.; Trucks, G. W.; Schlegel, H. B.; Gill, P. M. W.; Johnson, B. G.; Robb, M. A.; Cheeseman, J. R.; Keith, T. A.; Petersson, G. A.; Montgomery, J. A.; Raghavachari, K.; Al-Laham, M. A.; Zakrzewski, V. G.; Ortiz, J. V.; Foresman, J. B.; Cioslowski, J.; Stefanov, B. B.; Nanayakkara, A.; Challacombe, M.; Peng, C. Y.; Ayala, P. Y.; Chen, W.; Wong, M. W.; Andres, J. L.; Replogle, E. S.; Gomperts, R.; Martin, R. L.; Fox, D. J.; Binkley, J. S.; Defrees, D. J.; Baker, J.; Stewart, J. J. P.; Head-Gordon, M.; Gonzalez, C.; Pople, J. A. *Gaussian 94*; Gaussian Inc.: Pittsburgh, PA, 1995.
(27) (a) Becke, A. D. *Phys. Rev. A* **1988**, *38*, 3098. (b) Becke, A. D. *J. Chem. Phys.* **1993**, *98*, 5648.
(28) Lee, C.; Yang, W.; Parr, R. G. *Phys. Rev. B* **1998**, *37*, 785.
(29) Vosko, S. H.; Wilk, L.; Nusair, M. *Can. J. Phys.* **1980**, *58*, 1200.
(30) Raghavachari, K.; Binkley, J. S.; Seeger, R.; Pople, J. A. *J. Chem. Phys.* **1980**, *72*, 650.
(31) Wachters, A. J. H. *J. Chem. Phys.* **1970**, *52*, 1033.

Table 1. Computed Bond Distances, Vibrational Frequencies, and Bond Dissociation Energies (BDE) for the MO^+ Complexes

MO^+	state	r(M−O) (Å)	vib freq (cm^{-1})	BDE (kcal/mol)	BDE_{exp} (kcal/mol)[b]
ScO^+	$^1\Sigma^+$	1.603	1095	156.1	165.1
TiO^+	$^2\Delta$	1.563	1146	155.1	159.8
VO^+	$^3\Sigma^-$	1.532	1160	137.2	138.1
CrO^+	$^4\Sigma^-$	1.573	830	81.3	85.3 ± 1.3
MnO^+	$^5\Sigma^+$	1.715	640	56.4	68 ± 3
FeO^+	$^6\Sigma^+$	1.632	850	75.2	81 ± 2
	$^4\Delta$	1.683	675	69.4	
CoO^+	$^5\Delta$	1.625	816	73.3	77 ± 2
	$^3\Pi$	1.719	644	49.9	
NiO^+	$^2\Sigma^-$	1.646	642	69.3	63 ± 3
	$^4\Sigma^-$	1.618	783	57.9	
CuO^+	$^3\Pi$	1.758	569	37.6	37
	singlet	1.706[a]	709[a]		
		1.725	658		

[a] Spin-restricted B3LYP calculations. [b] Data from ref 16.

1.29 for Ni, and 1.44 for Cu)[32] resulting in a (611111111|51111|311|1)-[9s5p3d1f] contraction was used for the transition-metal ions. The spin-unrestricted version of the B3LYP (UB3LYP) method was applied even to singlet states when the reaction species are reasonably considered to have an open-shell-singlet electronic configuration. Computed $\langle S^2 \rangle$ values suggested that no spin contamination is included in the calculations,[33] except in open-shell-singlet calculations. Systematic frequency calculations were performed to characterize stationary points obtained and to take corrections of zero-point vibrational energy into account. Orbital interaction analyses based on the extended Hückel method[34] were carried out with YAeHMOP.[35] This approximate molecular orbital method should model reasonably well the general orbital energy trends, orbital interactions, and major charge shifts.

Results and Discussion

Electronic Structure of the MO^+ Complexes. Let us begin by looking at the general electronic features of the MO^+ complexes and the reliability of the energetics computed with a combination of the B3LYP method and the basis sets mentioned above. Carter and Goddard[36] predicted the bonding characters of the MO^+ complexes from generalized valence bond calculations. The metal−oxo bond and its catalytic function are significantly dependent on how the d-block orbitals are occupied; an early-transition-metal ion M^+ forms a strong, unreactive triple bond with an oxygen atom and a late-transition-metal ion forms a weak, reactive double bond with biradical character. The reactivity manifold of FeO^+, CoO^+, NiO^+, and CuO^+ has been investigated from DFT computations.[37]

Table 1 lists computed bond lengths and bond dissociation energies of the ground states of the MO^+ complexes. We can derive a general conclusion that the M−O distance increases with an increase in the number of d-electrons and its dissociation energy decreases with an increase in d-electrons. Scheme 1 shows the molecular orbitals of MO^+ which can be partitioned into bonding (2σ and 1π), nonbonding (1σ and 1δ), and antibonding (2π and 3σ) block orbitals. ScO^+, FeO^+, and CuO^+ can be formally viewed as d^0, $d,^5$ and d^8 complexes, respectively. In the $^1\Sigma^+$ ground state of ScO^+, four pairs of electrons occupy

Scheme 1

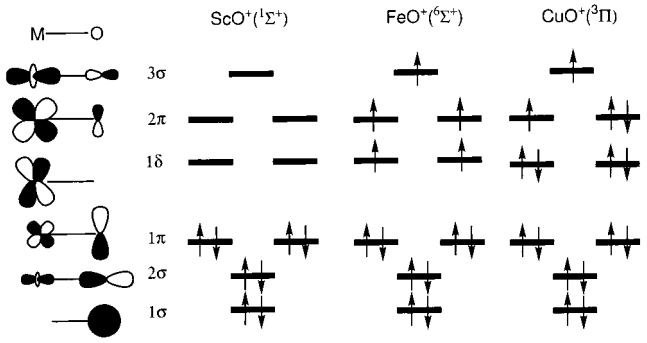

the nonbonding 1σ orbital and the three bonding orbitals to form a strong triple bond. Thus, ScO^+ is analogous to dinitrogen. At the B3LYP level of theory, the dissociation energy of ScO^+ is 156.1 kcal/mol relative to the dissociation limit of the ^{3}D state of Sc^+ and the ^{3}P state of O. This large dissociation energy is clearly a direct consequence of the three bonding orbitals that are fully occupied. The electronic features of TiO^+ and VO^+ are similar to that of ScO^+; although the nonbonding 1δ set that has no direct effect on the metal−oxygen bond is partly occupied, the three bonding orbitals are also fully occupied. Along the lines that such qualitative discussions suggest, our DFT calculations predicted that TiO^+ and VO^+ have comparable bond dissociation energies, 155.1 kcal/mol for TiO^+ and 137.2 kcal/mol for VO^+. Thus, each early MO^+ complex has a very strong triple bond, and accordingly the reactivities of these complexes toward inert alkanes are reasonably predicted to be low.

Let us next turn our attention to the electronic features of the late MO^+ complexes (FeO^+, CoO^+, NiO^+, and CuO^+). In the ground high-spin states of FeO^+, CoO^+, and NiO^+, all the bonding orbitals are doubly occupied and each 2π orbital is singly occupied; therefore they may resemble triplet dioxygen in the electronic configurations.[36] A computed dissociation energy for the $^6\Sigma^+$ state of FeO^+ (75.2 kcal/mol) at the B3LYP/6-311G** level is in good agreement with an experimental value of 81 ± 2 kcal/mol, that of the $^5\Delta$ state of CoO^+ (73.3 kcal/mol) is fully consistent with an experimental value of 77 ± 2 kcal/mol, and that of the $^4\Sigma^-$ state of NiO^+ (69.3 kcal/mol) is also in good agreement with an experimental value of 63 ± 3 kcal/mol.[12] A computed bond dissociation energy in the $^3\Pi$ ground state of CuO^+ is 37.6 kcal/mol, being also in excellent agreement with an experimental value of 37 kcal/mol.[16] In contrast to the early MO^+ complexes, there are low-lying excited (low-spin) states in the FeO^+, CoO^+, NiO^+, and CuO^+ complexes. Our calculations suggest that there are crossing regions of the high-spin and the low-spin potential energy surfaces.[18b] Spin inversion that can occur near a crossing region of potential energy surfaces of different spin states has a significant effect on the reactivity of these late MO^+ complexes toward methane, as discussed later in this article.

The FeO^+, CoO^+, and NiO^+ complexes are able to convert methane to methanol while the ScO^+, TiO^+, and VO^+ exhibit no direct reactivity toward small alkanes and alkenes. Bridging these extremes in the reactivity are the CrO^+ and MnO^+ complexes, which can be formally viewed as d^3 and d^4 complexes, respectively. In fact, the CrO^+ complex oxidizes saturated hydrocarbons larger than methane,[13c] and the MnO^+ complex activates the C−H bonds of methane giving rise to a CH_3 radical and not to methanol.[14d] As listed in Table 1, the bond dissociation energies of the CrO^+ and MnO^+ complexes are much smaller than those of the early MO^+ complexes that

(32) Raghavachari, K.; Trucks, G. W. *J. Chem. Phys.* **1989**, *91*, 1062.
(33) Wang, J.; Becke, A. D.; Smith, V. H., Jr. *J. Chem. Phys.* **1995**, *102*, 3477.
(34) (a) Hoffmann, R. *J. Chem. Phys.* **1963**, *39*, 1397. (b) Hoffmann, R.; Lipscomb, W. N. *J. Chem. Phys.* **1962**, *36*, 2179. (c) Hoffmann, R.; Lipscomb, W. N. *J. Chem. Phys.* **1962**, *37*, 2872.
(35) Landrum, G. A. *YAeHMOP "Yet Another extended Hückel Molecular Orbital Package"*; version 2.0, Cornell University: Ithaca, NY, 1997.
(36) Carter, E. A.; Goddard, W. A., III *J. Phys. Chem.* **1988**, *92*, 2109.
(37) Fiedler, A.; Schröder, D.; Shaik, S.; Schwarz, H. *J. Am. Chem. Soc.* **1994**, *116*, 10734.

Table 2. Calculated Atomic Charges and Spin Densities for the MO^+ Complexes from the Mulliken Population Analysis[a]

		atomic charge		atomic spin density	
MO^+	state	M	O	M	O
ScO^+	$^1\Sigma^+$	1.41 (1.78)	−0.41 (−0.78)	0.00	0.00
TiO^+	$^2\Delta$	1.36 (1.36)	−0.36 (−0.36)	1.14	−0.14
VO^+	$^3\Sigma^-$	1.31 (1.45)	−0.31 (−0.45)	2.33	−0.33
CrO^+	$^4\Sigma^-$	1.24 (1.35)	−0.24 (−0.35)	3.65	−0.65
MnO^+	$^5\Sigma^+$	1.35 (1.58)	−0.35 (−0.58)	4.75	−0.75
FeO^+	$^6\Sigma^+$	1.34 (1.46)	−0.34 (−0.46)	3.86	1.14
	$^4\Delta$	1.32 (1.42)	−0.32 (−0.42)	3.62	−0.63
CoO^+	$^5\Delta$	1.29 (1.38)	−0.29 (−0.38)	2.68	1.32
	$^3\Pi$	1.28 (1.32)	−0.28 (−0.32)	2.61	−0.61
NiO^+	$^4\Sigma^-$	1.23 (1.29)	−0.23 (−0.29)	1.53	1.47
	$^2\Sigma^-$	1.19 (1.34)	−0.19 (−0.34)	−0.23	1.23
CuO^+	$^3\Pi$	1.26 (1.32)	−0.26 (−0.32)	0.47	1.47
	singlet	1.21 (1.27)[b]	−0.21 (−0.27)[b]	0.00[b]	0.00[b]
		1.16 (1.21)	−0.16 (−0.21)	0.00	0.00

[a] Values in the parentheses are from natural population analysis. [b] Spin-restricted B3LYP calculations.

Table 3. Overall Energies for the Reactions, $MO^+ + CH_4 \rightarrow M^+ + CH_3OH$, at the B3LYP Level of Theory

	MO^+(spin state)	M^+(spin state)	ΔE_{calc} (kcal/mol)	ΔE_{exp} (kcal/mol)[a]
Sc	singlet	triplet	73.5	90.1 ± 1.6
Ti	doublet	quartet	72.4	84.4 ± 2.7
V	triplet	quintet	54.5	58.78 ± 2.7
Cr	quartet	sextet	−1.3	−3.0 ± 3.3
Mn	quintet	septet	−26.2	−23.9 ± 3.5
Fe	quartet	sextet	−12.6	−8.2 ± 1.6
Co	triplet	triplet	−25.6	−14.7 ± 1.6
Ni	doublet	doublet	−26.5	−28.6 ± 1.9
Cu	singlet	triplet	−50.0	−60.1 ± 4.1

[a] Data from ref 15a.

exceed 100 kcal/mol. Computed and experimental bond dissociation energies for CrO^+ and MnO^+ are in excellent agreement.

Table 2 summarizes computed Mulliken atomic charges and spin densities of the MO^+ complexes. The Mulliken population analysis is known to have several limitations;[38] those of the metals lie in a region from 1.2 to 1.4 in most cases while the formal charges are +3 for all, and those of oxygen lie in a region from −0.2 to −0.4 while the formal charge is −2. The natural population analysis[39] gave values similar to the Mulliken atomic charges, as indicated by the parentheses in Table 2. The formal charge +3 is usual for Sc, Ti, V, Cr, Mn, Fe, Co, and Ni. It is rare for Cu, but high-oxidation-state Cu(III) ions have been increasingly recognized as a biologically important species in copper proteins. Moreover, Table 2 shows that the spin density on the O atom, which can be determined by the occupancy of the 2π and 3σ orbitals, significantly increases when the number of d-electrons increases. Computed spin densities on the O atoms of the high-spin states of FeO^+, CoO^+, NiO^+, and CuO^+ are more than unity. Since the spin density is likely to have relevance to the reactivity of the MO^+ complexes, we can qualitatively predict that the late MO^+ complexes should have significant ability to activate the C−H bonds of methane.

Table 3 lists computed and measured overall energies for the reactions, $MO^+ + CH_4 \rightarrow M^+ + CH_3OH$, our DFT computations being in excellent agreement with experimental estimations by Armentrout et al.[15a] In summary of this section, we conclude that the B3LYP method coupled with the 6-311G** basis set behaves nicely for the prediction of the electronic properties and the reactivities of the bare MO^+ complexes. Our method of choice is therefore appropriate for the purpose of the present study.

Scheme 2

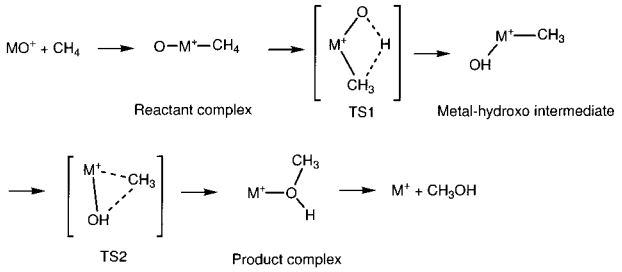

Table 4. Geometrical Parameters of TS1s in Units of Å

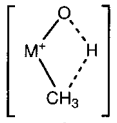

MO^+	spin state	r(M−C)	r(C−H)	r(H−O)	r(M−O)	r(M−H)
ScO^+	singlet	2.255	1.483	1.250	1.699	1.822
TiO^+	doublet	2.205	1.541	1.219	1.656	1.781
VO^+	triplet	2.134	1.567	1.214	1.624	1.748
CrO^+	quartet	2.121	1.413	1.293	1.634	1.769
MnO^+	quintet	2.134	1.313	1.397	1.647	1.777
FeO^+	sextet	2.171	1.426	1.304	1.717	1.781
	quartet	2.084	1.325	1.383	1.619	1.751
CoO^+	quintet	2.162	1.463	1.273	1.703	1.765
	triplet	2.110	1.276	1.404	1.657	1.791
NiO^+	quartet	2.097	1.406	1.308	1.792	1.789
	doublet	2.033	1.240	1.499	1.643	1.784
CuO^+	triplet	2.079	1.388	1.312	1.830	1.790
	singlet	2.123	1.230	1.445	1.750	1.889

Reactivity of MO^+ toward CH_4. The concerted reaction pathway for the direct methane−methanol conversion by MO^+ can be partitioned into the first H atom abstraction step via TS1 and the second methyl migration step via TS2, as indicated in Scheme 2.[18] We will compare the reactivities of various MO^+ complexes with respect to the ability to activate the strong C−H bonds of methane. We would like to systematically explain from computed energetics for the reaction species of various transition metals how the reactivity changes as a function of the number of d-electrons in these complexes. Optimized geometrical parameters of the four-centered TS1s, the metal−hydroxo intermediates, and the three-centered TS2s are listed in Tables 4, 5, and 6, respectively. The first transition state TS1 is related to the most important electronic process that is responsible for the C−H bond dissociation of methane. Figure 1 presents the histograms of computed activation energies for the H-atom abstraction of methane in the MO^+/CH_4 systems. The indicated relative energies are measured in two ways: (a) from the reactant complex $OM^+(CH_4)$ of the ground state (ΔE_1) and (b) from the dissociation limit of the ground-state $MO^+ + CH_4$ (ΔE_2). MnO^+ exhibits a ΔE_1 value of only 9 kcal/mol, but the other MO^+ complexes have ΔE_1 values falling in a range of 20−35 kcal/mol. One should note that TS1s of the low-spin states lie in general below those of the high-spin states for FeO^+, CoO^+, and NiO^+. Our calculations suggest that the C−H bond dissociations via TS1s for FeO^+, CoO^+, and NiO^+ should occur with spin-inversion in the vicinity of a crossing region of the high-spin and the low-spin potential energy surfaces. This is

(38) (a) Hall, G. G. *Adv. Atom Mol. Phys.* **1985**, *20*, 41. (b) Huzinaga, S.; Sakai, Y.; Miyoshi, E.; Narita, S. *J. Chem. Phys.* **1990**, *93*, 3319.

(39) (a) Carpenter, J. E.; Weinhold, F. *J. Mol. Struct.* (*Theochem*) **1988**, *169*, 41. (b) Glendening, E. D.; Reed, A. E.; Carpenter, J. E.; Weinhold, F. NBO, Version 3.1.

Table 5. Geometrical Parameters of the Metal−Hydroxo Intermediates in Units of Å and deg

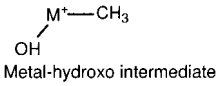

Metal-hydroxo intermediate

MO^+	spin state	r(M−C)	r(M−O)	θ(C−M-O)
ScO^+	singlet	2.102	1.774	107.6
TiO^+	doublet	2.032	1.718	108.1
VO^+	triplet	1.978	1.691	109.4
CrO^+	quartet	1.967	1.700	138.6
MnO^+	quintet	1.971	1.722	109.2
FeO^+	sextet	1.961	1.730	141.7
	quartet	1.950	1.696	109.7
CoO^+	quintet	1.946	1.717	156.9
	triplet	1.900	1.693	106.2
NiO^+	quartet	2.011	1.708	141.6
	doublet	1.875	1.677	104.1
CuO^+	triplet	1.993	1.776	168.0
	singlet	1.727	1.892	94.7

Table 6. Geometrical Parameters of TS2s in Units of Å

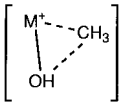

TS2

MO^+	spin state	r(M−C)	r(C−O)	r(M−O)
ScO^+	triplet	2.755	1.938	1.896
	singlet	2.824	1.907	1.850
TiO^+	quartet	2.653	2.014	1.864
	doublet	2.766	1.939	1.830
VO^+	quintet	2.765	1.939	1.830
	triplet	2.507	1.991	1.842
CrO^+	sextet	2.297	2.064	1.859
	quartet	2.541	1.984	1.827
MnO^+	septet	3.178	2.503	1.801
	quintet	2.563	2.056	1.826
FeO^+	sextet	3.038	2.371	1.771
	quartet	2.434	2.020	1.792
CoO^+	quintet	2.495	2.189	1.818
	triplet	2.284	2.001	1.783
NiO^+	quartet	2.402	2.183	1.837
	doublet	2.123	1.961	1.801
CuO^+	triplet	2.424	2.120	1.826
	singlet	1.992	2.112	1.774

included in the ΔE_1 values. As a consequence, the ΔE_1 values for FeO^+ and NiO^+ are measured to be 22.1 and 25.3 kcal/mol, respectively. Since the ΔE_1 value for ScO^+ is 25.8 kcal/mol, the reactivity of ScO^+ toward methane should be similar to that of NiO^+ of the low-spin state. However, the ScO^+ complex cannot react with methane, and the reaction efficiency is less than 0.01%, whereas that of NiO^+ is 20%, thus the calculations and the experimental values not being consistent. Thus, ΔE_1 is not a good reactivity index for the methane activation by MO^+ in the gas phase. The internal energy of the reacting system is increased during the formation of the reactant complex, and it can be used for the C−H bond activation of methane. Concerning the gas-phase reaction in the adiabatic environment, the barrier height of TS1 relative to the dissociation limit (ΔE_2) may be a substantial activation barrier to be considered. In fact, computed ΔE_2 values are negative for the low-spin states of CrO^+, MnO^+, FeO^+, and NiO^+ and for both high-spin and low-spin states of CuO^+. These results are fully consistent with the experimental observations that MnO^+, FeO^+, and NiO^+ efficiently activate methane. Thus, ΔE_2 is probably a better reactivity index. We expect from the negative ΔE_2 values that methane should be effectively activated by CrO^+, MnO^+, FeO^+, NiO^+, and CuO^+, especially on the low-spin potential energy surfaces. The triplet state of TS1 in the CuO^+/CH_4 system also lies below the dissociation limit by 13.0 kcal/mol. We therefore predict that CuO^+ should exhibit very high ability for methane oxidation; however, the reaction between CuO^+ and methane has not yet been observed because CuO^+ itself is not stable under ICR conditions due to the weak Cu−O bond.

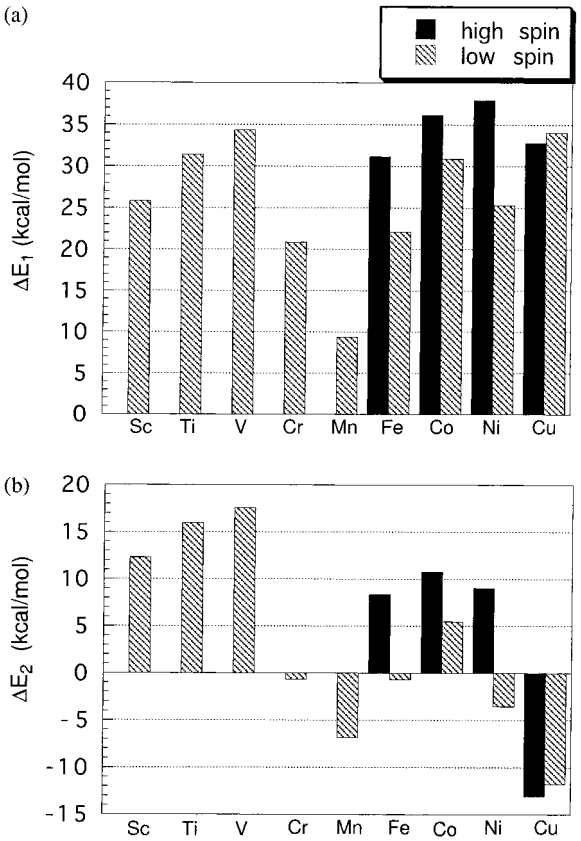

Figure 1. Computed potential energy profiles for the H atom abstraction of methane in the MO^+/CH_4 system. The relative energies (ΔE_1 and ΔE_2) are measured from (a) a reactant complex, $OM^+(CH_4)$, of the ground state and (b) a dissociation limit, $MO^+ + CH_4$, of the ground state.

Possible Conversion of Methane to Methanol by ScO^+, TiO^+, and VO^+. Having described the general features of the reactivities of the MO^+ complexes, let us look at the detailed profiles of computed energy diagrams for the possible methane hydroxylation by the early MO^+ complexes. Experiments carried out in Schwarz's group have shown that these early transition-metal oxide ions hardly react with methane, the reaction efficiencies being less than 0.01%.[16] The computed energy profiles are uphill toward the product direction, as shown in Figure 2, so the computational result is qualitatively consistent with the experimental result. Another possible restriction to these reactions is the spin-forbidden electronic process. The reactants (ScO^+ ($^1\Sigma^+$), TiO^+ ($^2\Delta$), and VO^+ ($^3\Sigma^-$) + CH_4) and the products (Sc^+ (^{3}D), Ti^+ (^{4}F), and V^+ (^{5}D) + CH_3OH) have different spin multiplicities in the ground states, and therefore the reaction pathways should involve a spin-inversion electronic process near a crossing region between the high-spin and the low-spin potential energy surfaces. Our calculations strongly suggest that this can actually occur in the vicinity of TS2.

The first step of the reaction is the formation of the reactant complex, OM^+-CH_4. Computed binding energies for OSc^+-CH_4, OTi^+-CH_4, and OV^+-CH_4 are 13.5, 15.4, and 16.8 kcal/

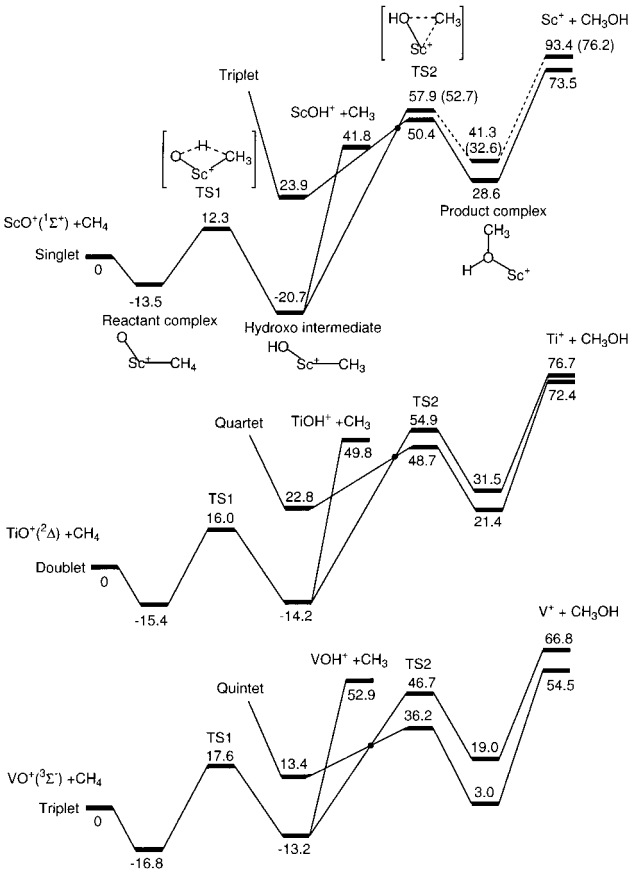

Figure 2. Potential energy diagrams (including zero-point energy) along the reaction pathway, $MO^+ + CH_4 \rightarrow M^+ + CH_3OH$, in the high-spin and the low-spin states. Relative energies are in kcal/mol. The dotted lines in the region of TS2, $Sc^+(CH_3OH)$, and Sc^+ indicate the use of the spin-unrestricted method. Values in parentheses are energies in the open-shell singlet.

mol, respectively. Thus, methane is strongly bound to these early complexes. The bound methane in the reactant complexes undergoes a concerted 1,3-hydrogen migration, forming the metal−hydroxo intermediate CH_3-M^+-OH on a single potential energy surface. The cleavage of a C−H bond of methane is an essential electronic process in the course of the reaction. The barrier height of TS1 measured from the dissociation limit (ΔE_2), which is a good measure for the ability of methane activation, as mentioned above, is 12.3, 16.0, and 17.6 kcal/mol on the ground-state potential energy surfaces for the ScO^+, TiO^+, and VO^+ complexes, respectively. The resultant metal−hydroxo intermediates are stable in energy; they lie 13−20 kcal/mol below the dissociation limits.

The second half of the reaction pathway is responsible for the formation of the product complex $MO^+(CH_3OH)$ that is formed in a concerted manner via TS2; this process can be viewed as a rebound step for the OH and CH_3 groups. We note that the singlet and triplet states are reversed in energy during these processes, as shown by the closed points on the energy diagrams in Figure 2. Thus, there should be a crossing of the low-spin and the high-spin potential energy surfaces. The product complexes are less stable in energy than the dissociation limits by 28.6, 21.4, and 3.0 kcal/mol in the ScO^+, TiO^+, and VO^+/CH_4 systems, respectively. The release of methanol requires high activation energy in each case. The overall reaction energies for ScO^+, TiO^+, and VO^+ are 73.5, 72.4, and 54.5 kcal/mol endothermic, respectively, if we take the spin inversion into account. As a consequence, the methane-to-methanol conversion by these early MO^+ complexes is not at all preferred in energy. The energetics of the energy diagrams is in good agreement with the experimental observations.

It is difficult to describe the singlet states of $Sc(CH_3OH)^+$ and Sc^+ within the framework of the spin-restricted method. In particular, since the Sc^+ ion should have a $3d^14s^1$ configuration, we cannot impose a closed-shell electronic configuration on such an open-shell system. We therefore carried out open-shell-singlet calculations for $Sc(CH_3OH)^+$ and Sc^+ with the spin-unrestricted version of the B3LYP method (UB3LYP) as well as closed-shell-singlet calculations. The energies in parentheses are the values obtained from such open-shell-singlet calculations. The open-shell-singlet potential energy surface lies always below the closed-shell-singlet potential energy surface, the calculated splitting being 5.2 kcal/mol in TS2, 8.7 kcal/mol in the product complex, and 17.2 kcal/mol in the Sc^+ ion. Unfortunately, the open-shell-singlet wave function is significantly spin-contaminated, but the energies from such calculations should be better than those from spin-restricted calculations.

We calculated another reaction branch indicated in eq 3, which leads to the decomposition into $M^+OH + {}^\bullet CH_3$. This is a side reaction from the viewpoint of methanol production. This is lower in energy than TS2 for the ScO^+ complex; thus, our DFT calculations show that the formation of methyl radical should be energetically more favorable than the formation of methanol. It is energetically comparable to TS2 for the TiO^+ complex and higher than TS2 for the VO^+ complex. Thus, the preference for methyl radical in the ScO^+/CH_4 system is reversed in the VO^+/CH_4 system. Ricca and Bauschlicher studied the M^+OH, $M^+(OH)_2$, and $M^+(OH)_3$ complexes theoretically from both B3LYP and CCSD(T) calculations,[40] the results from the two methods being in good agreement.

$$CH_3-M^+-OH \rightarrow MOH^+ + {}^\bullet CH_3 \qquad (4)$$

The conversion of methanol to methane by the Sc^+, Ti^+, and V^+ ions is clearly more favorable in energy than the methane to methanol conversion in view of the potential energy diagrams in Figure 2. Thus, the early-transition metals behave as a good oxygen acceptor for methanol. Irigoras, Fowler, and Ugalde recently carried out ab initio calculations for the analogous electronic processes, $M^+ + H_2O \rightarrow MO^+ + H_2$, where M is Sc to Cu.[41]

Conversion of Methane to Methanol by CrO^+ and MnO^+. Let us next look at the reactions of CrO^+ and MnO^+ with methane. The CrO^+ and MnO^+ complexes are the bridging between the early- and the late-transition MO^+ complexes, as mentioned above. Figure 3 shows a computed potential energy diagram along the methane hydroxylation pathway, $CrO^+ + CH_4 \rightarrow Cr^+ + CH_3OH$, in the quartet and the doublet states. Kang and Beauchamp investigated the gas-phase reactions of CrO^+ with alkanes,[13c] and demonstrated that CrO^+ is able to convert ethane to ethanol without formation of a byproduct. Since the high-spin sextet potential energy surface lies above the low-spin quartet one in the entrance channel, but this is reversed in the exit channel, a crossing between the sextet and the quartet potential energy surfaces should occur once in the

(40) Ricca, A.; Bauschlicher, C. W., Jr. *J. Phys. Chem. A* **1997**, *101*, 8949.

(41) (a) Irigoras, A.; Ugalde, J. M.; Lopez, X.; Sarasola, C. *Can. J. Chem.* **1996**, *74*, 1824. (b) Irigoras, A.; Fowler, J. E.; Ugalde, J. M. *J. Phys. Chem. A* **1998**, *102*, 293. (c) Irigoras, A.; Fowler, J. E.; Ugalde, J. M. *J. Am. Chem. Soc.* **1999**, *121*, 574. (d) Irigoras, A.; Elizalde, O.; Silanes, I.; Fowler, J. E.; Ugalde, J. M. *J. Am. Chem. Soc.* **2000**, *122*, 114.

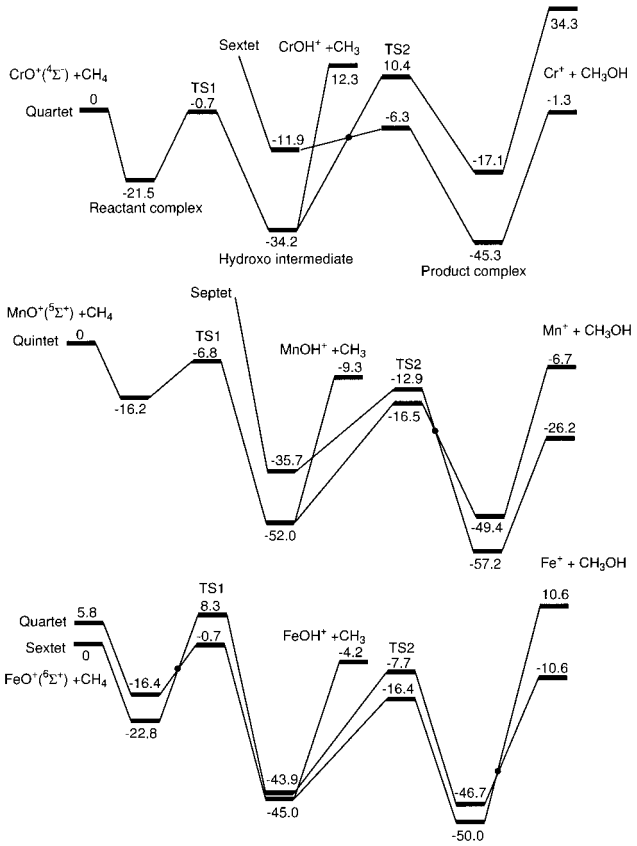

Figure 3. Potential energy diagrams (including zero-point energy) along the reaction pathway, $MO^+ + CH_4 \rightarrow M^+ + CH_3OH$, in the high-spin and the low-spin states. Relative energies are in kcal/mol.

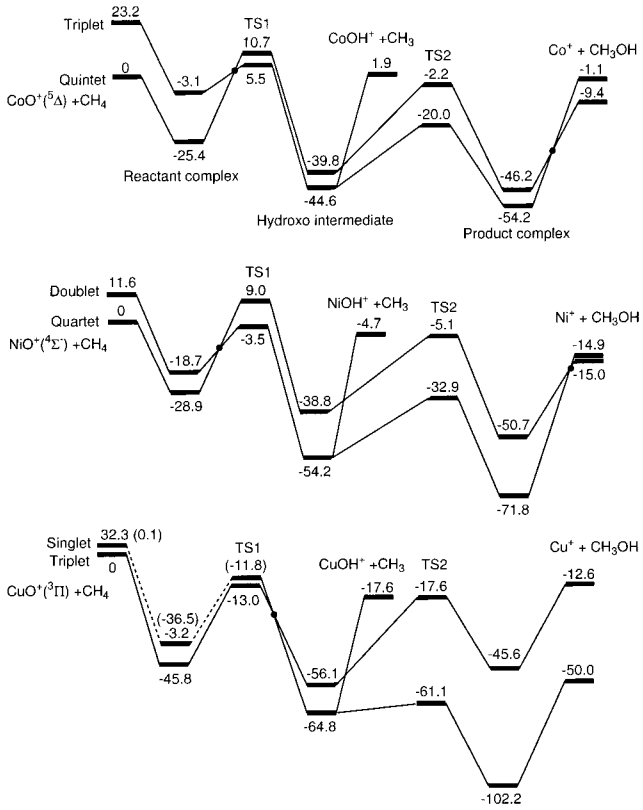

Figure 4. Potential energy diagrams (including zero-point energy) along the reaction pathway, $MO^+ + CH_4 \rightarrow M^+ + CH_3OH$, in the high-spin and the low-spin states. Relative energies are in kcal/mol. The dotted lines in the region of CuO^+, $CuO^+(CH_4)$, and TS1 indicate the use of the spin-unrestricted method. Values in parentheses are energies in the open-shell singlet.

course of the reaction. Thus, only the quartet state plays an essential role in the first half of the reaction pathway. TS1 for CrO^+ is very different from those for ScO^+, TiO^+, and VO^+ because it lies 0.7 kcal/mol below the dissociation limit $CrO^+ + CH_4$. Since the initial potential energy is large enough for passing over TS1, the reactivity of CrO^+ is expected to be higher than those of the early MO^+ complexes with respect to the C−H bond activation. The hydroxo intermediate CH_3-Cr^+-OH of the quartet state was calculated to be −34.2 kcal/mol measured from the dissociation limit. The simple electronic process that breaks the Cr−C bond in the hydroxo intermediate leads to the formation of byproducts $CrOH^+ + {}^\bullet CH_3$. Its energetics is considerably high compared to that of TS2. Thus, the dissociation into $CrOH^+ + {}^\bullet CH_3$ should be energetically unfavorable compared to the reaction pathway toward the product complex $Cr^+(CH_3OH)$.

The energy diagram of the quartet state lies below that of the sextet state in the first half of the reaction pathway, but the relative order is reversed in the vicinity of TS2. Thus, this possible spin inversion should greatly affect the reaction pathway. The conversion of methane to methanol is 34.3 kcal/mol endothermic if the reaction proceeds on the quartet potential energy surface as a spin-conserving process, whereas it is 1.3 kcal/mol exothermic if the spin inversion takes place in the vicinity of TS2. Armentrout et al. estimated from an ion beam experiment that the overall reaction is 4 kcal/mol exothermic;[15a] therefore this nonadiabatic process is strongly suggested to occur in the possible methane hydroxylation by CrO^+.

Schröder, Schwarz, and collaborators reported that MnO^+ reacts with methane in the quintet ground state[14d] and demonstrated that the formation of $MnOH^+ + {}^\bullet CH_3$ is a main process while the formation of methanol is a minor branch. Figure 3 shows a computed potential energy diagram along the reaction pathway, $MnO^+ + CH_4 \rightarrow Mn^+ + CH_3OH$, in the quintet and septet states. The activation energy for the C−H bond dissociation via TS1 is −6.8 kcal/mol measured from the dissociation limit. Thus, this electronic process is energetically preferred, which is consistent with an observed reaction efficiency of 40%. Thus, the excellent agreement between theory and experiment shows that the barrier height of TS1 is directly relevant to the reaction efficiency of MO^+ toward methane. We will consider in the next section why the methanol branching ratio is low in the reaction between MnO^+ and methane.

Conversion of Methane to Methanol by FeO^+, CoO^+, and NiO^+. These late MO^+ complexes are able to convert methane to methanol under ICR conditions, but their reaction efficiencies and methanol branching ratios are very different.[16] Let us consider the reactions of FeO^+, CoO^+, and NiO^+ with methane; the energy diagrams for the reaction pathways are presented in Figures 3 and 4. The general profiles of these diagrams are quite similar, but the small differences can determine the observed different reaction efficiencies and methanol branching ratios. A low-energy reaction pathway for the methane-to-methanol conversion by FeO^+, CoO^+, and NiO^+ is opened in the entrance channel by a crossing of the high-spin and the low-spin potential energy surfaces. There is another surface crossing in the exit channel. Thus, spin inversion is very likely to occur twice along the entire reaction pathway, which is the most important aspect in the reactions of FeO^+, CoO^+, and NiO^+ with methane. Such behavior is not observed in the reactions by the other MO^+ complexes. This is good for the conversion of methane to

Table 7. Measured Reaction Efficiencies and Product Branching Ratios for the Reaction of MO^+ with Methane[16]

MO^+	ϕ	$MOH^+ + CH_3$	$MCH_2^+ + H_2O$	$M^+ + CH_3OH$
MnO^+	40	100		<1
FeO^+	20	57	2	41
CoO^+	0.5			100
NiO^+	20			100

methanol from the viewpoint of catalytic function in that the initial spin state is conserved in a single catalytic cycle.

In the FeO^+/CH_4 system, TS1 of the sextet state lies 8.3 kcal/mol above the dissociation limit, while TS1 of the quartet state lies −0.7 kcal/mol below the dissociation limit when spin inversion takes place from the sextet state to the quartet state. Thus, such a nonadiabatic electronic process can provide a low-energy reaction pathway for the C−H bond cleavage process. Similar crossings are seen for the CoO^+ and NiO^+ systems. In the NiO^+/CH_4 system, TS1 of the quartet spin state lies 9.0 kcal/mol above the dissociation limit, while TS1 of the doublet spin state lies −3.5 kcal/mol below the dissociation limit when spin inversion takes place. Thus, the ΔE_2 values are −0.7 and −3.5 kcal/mol for FeO^+ and NiO^+, respectively. In contrast to FeO^+ and NiO^+, the ΔE_2 value in the CoO^+/CH_4 system is 5.5 kcal/mol even if we take the spin inversion into account.

As listed in Table 7, the observed reaction efficiencies of MnO^+, FeO^+, CoO^+, and NiO^+ toward methane are 40, 20, 0.5, and 20%, respectively.[16] Thus, our calculations can successfully explain the general features of the experimental observations that the reactivities of MnO^+, FeO^+, and NiO^+ are higher than that of CoO^+. This table tells us that MnO^+ activates methane very efficiently, but the main reaction is unfortunately the formation of methyl radical. In contrast, although the reaction efficiency of CoO^+ toward methane is very low, the branching ratio to methanol is 100%. FeO^+ exhibits intermediate features in both reaction efficiency and branching ratio, and NiO^+ is a very good mediator for the conversion of methane to methanol. The reaction efficiency is most likely to have relevance to the barrier height of TS1, which is best represented by ΔE_2 in Figure 1. Our computational results and the experimental observations are in excellent agreement; computed ΔE_2 values (observed reaction efficiencies) for MnO^+, FeO^+, CoO^+, and NiO^+ are −6.8 l (40%), −0.7 (20%), 5.5 (0.5%), and −3.5 kcal/mol (20%), respectively. These results clearly show that the formation of the metal−hydroxo intermediate is the key step for methane activation.

The barrier heights of TS2 measured from the dissociation limit (ΔE_3), which should determine the methanol branching ratio, are −16.5, −16.4, −20.0, and −32.9 kcal/mol for MnO^+, FeO^+, CoO^+, and NiO^+, respectively. Since these values are lower in energy than those of TS1, the rate-determining step in the two-step concerted mechanism in Scheme 2 is the first electronic process that is responsible for the C−H bond dissociation. The methanol branching ratios to methanol are 100% for CoO^+ and NiO^+, 41% for FeO^+, and <1% for MnO^+. Unfortunately, one cannot explain the methanol branching ratios only from the barrier heights of TS2. Methyl radical is a competitive byproduct in the conversion of methane to methanol, and it is essential to consider the methyl radical formation pathway as another reaction branch. The total energy of $MOH^+ + {}^\bullet CH_3$ measured from the dissociation limit (ΔE_4) is −9.3, −4.2, 1.9, −4.7 kcal/mol for M = Mn, Fe, Co, and Ni, respectively. However, these values do not exactly reflect the experimental observations for the methanol branching ratios summarized in Table 7. What is a better criterion for estimating the preference of the methanol formation pathway? If the value of $\Delta E_3 - \Delta E_4$ is large and negative, we can reasonably conclude that the methanol branching ratio is energetically preferred. This quantity is −7.2, −12.2, −21.9, and −28.2 kcal/mol for MnO^+, FeO^+, CoO^+, and NiO^+, respectively. This result clearly demonstrates that the methanol formation pathway is energetically preferred in CoO^+ and NiO^+, that the methyl radical formation pathway is preferred in MnO^+, and that the two reaction pathways are competitive in FeO^+. Thus, the value of $\Delta E_3 - \Delta E_4$ is a very good measure in predicting the preference of the methanol formation pathway.

Table 8. Computed Total Energies of $MOH^+ + CH_3{}^\bullet$ and of $MOH + CH_3^+$ Measured from the Dissociation Limits of $MO^+ + CH_4$

$MOH^+ + CH_3{}^\bullet$	energy (kcal/mol)	$MOH + CH_3^+$	energy (kcal/mol)
$^2ScOH^+ + {}^\bullet CH_3$	41.8	$^1ScOH + CH_3^+$	130.3
$^3TiOH^+ + {}^\bullet CH_3$	49.8	$^2TiOH + CH_3^+$	166.2
$^4VOH^+ + {}^\bullet CH_3$	52.9	$^3VOH + CH_3^+$	149.1
$^5CrOH^+ + {}^\bullet CH_3$	12.3	$^4CrOH + CH_3^+$	95.3
$^6MnOH^+ + {}^\bullet CH_3$	−9.3	$^5MnOH + CH_3^+$	62.6
		$^7MnOH + CH_3^+$	70.4
$^5FeOH^+ + {}^\bullet CH_3$	−4.2	$^6FeOH + CH_3^+$	71.6
		$^4FeOH + CH_3^+$	61.1
$^4CoOH^+ + {}^\bullet CH_3$	1.9	$^5CoOH + CH_3^+$	72.4
		$^3CoOH + CH_3^+$	58.1
$^3NiOH^+ + {}^\bullet CH_3$	−4.7	$^4NiOH + CH_3^+$	66.6
		$^2NiOH + CH_3^+$	47.0
$^2CuOH^+ + {}^\bullet CH_3$	−17.6	$^3CuOH + CH_3^+$	52.4

The formation of methyl cation is a possible competing reaction and we considered the energetics of the reaction indicated by eq 5.

$$CH_3{-}M^+{-}OH \rightarrow MOH + CH_3{}^+ \qquad (5)$$

The total energies of $MOH + CH_3^+$ are more than 50 kcal/mol higher than those of $MOH^+ + {}^\bullet CH_3$, as listed in Table 8. We can therefore rule out the occurrence of this side reaction in the gas phase.

Conversion of Methane to Methanol by CuO^+. Let us finally look at the reaction pathway of $CuO^+ + CH_4 \rightarrow Cu^+ + CH_3OH$. Unfortunately, experimental information is not available for this reaction at present. The energy diagram for the methane hydroxylation shown in Figure 4 is downhill toward the product direction. Thus, CuO^+ is likely to be a very good mediator for this electronic process. The ground state of CuO^+ is a triplet and that of Cu^+ is a singlet, and therefore spin inversion from the triplet state to the singlet state is expected to occur once in the course of the reaction; the energy diagram suggests that it is most likely to occur after TS1. Since TS1 of the triplet state lies 13 kcal/mol below the dissociation limit, we expect that the C−H bond dissociation of methane should take place at no cost of activation energy. This process is a spin-conserving reaction on the triplet potential energy surface, which is in remarkable contrast to those of the other late MO^+ complexes (FeO^+, CoO^+, and NiO^+) since these complexes exhibit the so-called two-state reactivity[22] during the C−H bond dissociation process. TS1 of the singlet state is found only by using the UB3LYP method, it lying 1.2 kcal/mol above TS1 of the triplet state. The energies in parentheses are the values obtained from such open-shell-singlet calculations. Since computed $\langle S^2 \rangle$ values of these open-shell singlet states are about 1, it is highly possible that the calculated energies are erroneously underestimated. The energy of TS2 relative to the dissociation limit was calculated to be −61.1 kcal/mol in the singlet state

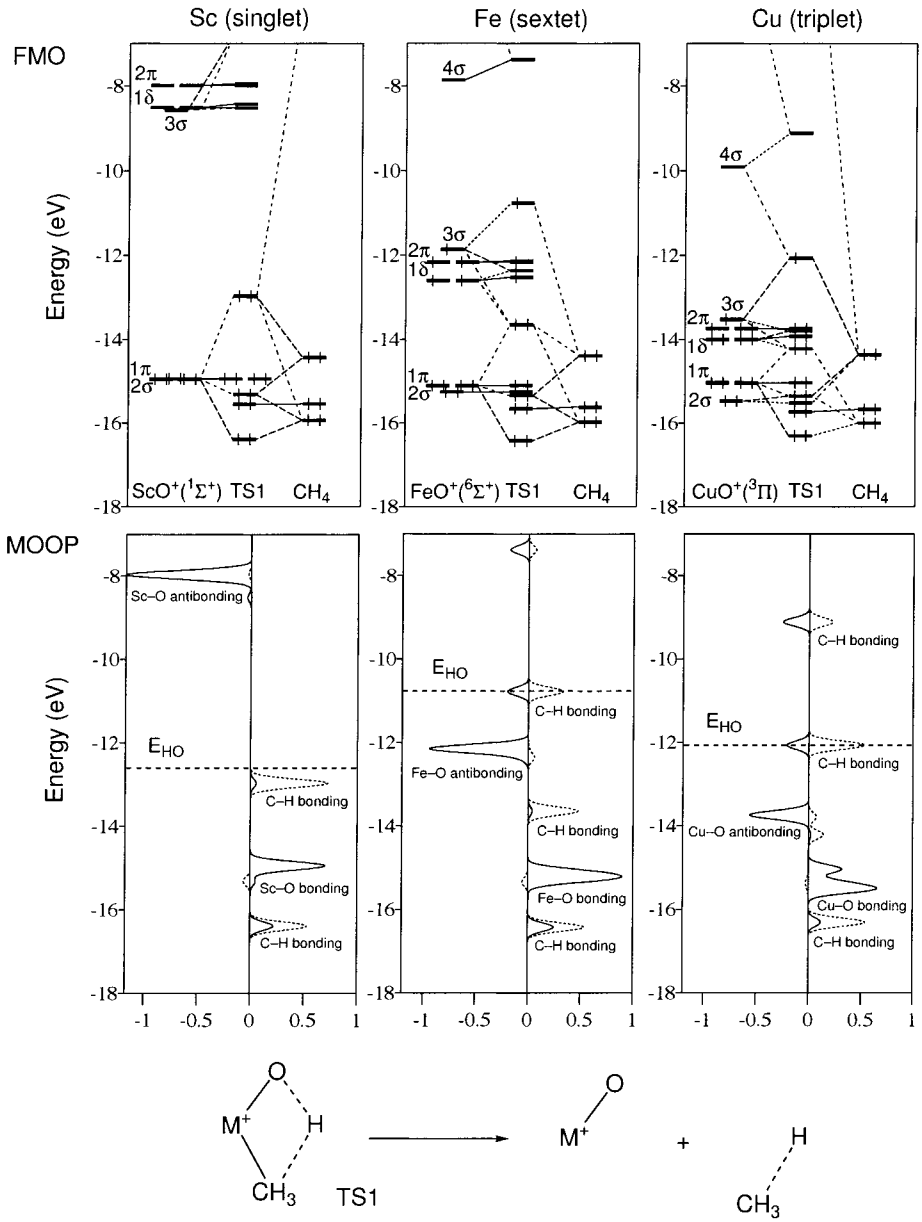

Figure 5. Fragment molecular orbital (FMO) and molecular orbital overlap population (MOOP) analyses of TS1 for the singlet state of ScO^+ (left), the sextet state of FeO^+ (center), and the triplet state of CuO^+ (right). Solid and dotted curves in MOOP indicate the contribution to the M−O bond and the C−H bond being dissociated, respectively.

and −17.6 kcal/mol in the triplet state. On the singlet potential energy surface, the barrier height of TS2 relative to the hydroxo intermediate is only 3.7 kcal/mol and that of the product complex is −102.2 kcal/mol. This reaction is therefore preferred from the point of view of energetics. The overall reaction is 50.0 kcal/mol exothermic with spin inversion from the triplet state to the singlet state. We thus conclude that the methane-to-methanol conversion should be best mediated by CuO^+.

Orbital Interaction Analyses. Why are the late MO^+ complexes relatively active to methane and other small alkanes? To gain a better understanding of the reactivities, we can derive useful information from fragment molecular orbital (FMO) and molecular orbital overlap population (MOOP) analyses[42] based on the extended Hückel method.[34] This method is reliable especially in orbital interaction analysis. Since spin-unrestricted methodologies can complicate orbital interactions, we prefer the qualitative molecular orbital method for the purpose of orbital interaction analysis. The most important step in the methane-to-methanol conversion by the MO^+ complexes is clearly the C−H bond dissociation via TS1. This electronic process can be qualitatively understood from simple molecular orbital ideas. Here we consider in Figure 5 why the orbital interactions in TS1 are changed in different transition-metal oxide ions. The spin multiplicities of ScO^+, FeO^+, and CuO^+ indicated in the illustrations are singlet, sextet, and triplet, respectively. In the FMO analyses, the orbital interactions are partitioned into MO^+ (ScO^+, FeO^+, and CuO^+) and CH_4 fragments; on the left the orbitals for the MO^+ fragment are shown and on the right the orbitals for the CH_4 fragment are shown. In the illustrations, the MO^+ fragments have high-lying d-block orbitals of 3σ, 1δ, and 2π and low-lying ligand orbitals of 2σ and 1π while the CH_4 fragment has three C−H bonding orbitals that derive from the 3-fold degenerate HOMO of T_d methane. We can reconstruct

(42) MOOP was introduced by D. M. Prosperio and C. Mealli, in CACAO (a package of programs for extended Hückel molecular orbital analysis).

the molecular orbitals of TS1 from these fragment molecular orbitals, as shown at the center of each FMO diagram.

The very high-lying d-block orbitals of the ScO^+ fragment and the C−H bonding orbitals have no net interaction; only the low-lying occupied ligand orbitals of ScO^+ interact with the C−H bonding orbitals. However, these are two-orbital-four-electron interactions, which can generally result in repulsion between two molecular fragments. Thus, ScO^+ is not effective for methane activation. On the other hand, the partially occupied d-block orbitals of the FeO^+ and CuO^+ fragments and the C−H bonding orbitals have significant interactions because the d-block orbitals of these are lower in energy than those of ScO^+. This is a remarkable difference between the early and the late MO^+ complexes. Since the d-block orbitals of FeO^+ and CuO^+ are not fully occupied, the orbital interactions can lead to energetical stabilization of the whole molecular systems, due to two-orbital-two-electron or two-orbital-three-electron interactions. The 3σ orbitals of FeO^+ and CuO^+ play an important role in the C−H bond activation of methane as expected, and we can derive an important result. TS1 of the low-spin quartet state for FeO^+ can be greatly stabilized in energy because the interaction between the 3σ orbital and the HOMO of the CH_4 fragment is of the two-orbital-two-electron type and the destabilized 3σ orbital at −10.7 eV is unoccupied in the low-spin state.[18c] This is the reason that TS1 in the FeO^+/CH_4 system prefers the low-spin quartet state to the high-spin sextet state. The d-block orbitals of CuO^+ and the C−H bonding orbitals of the CH_4 fragment are highly correlated, and the reconstructed orbitals for TS1 are low-lying in energy. In particular, the interaction between the 3σ orbital of CuO^+ and the HOMO of the CH_4 fragment is significant. It is thus reasonable from the viewpoint of one-electron approximation that TS1 for CuO^+ is energetically stable.

In addition to the FMO analyses, we carried out MOOP analyses to look in detail at how the C−H bond of methane is cleaved through the formation of TS1. The MOOP diagrams in Figure 5b show graphically the contribution of various molecular orbitals to the overlap populations. Solid and dotted curves indicate the contributions of the M−O bond and the C−H bond being dissociated, respectively. The dotted horizontal lines indicate the highest level occupied by one or two electrons in certain spin states. Bonding overlap populations are plotted to the right and antibonding ones are plotted to the left. The HOMO and the HOMO-2 of the CH_4 fragment have positive values of overlap population while the 2π orbitals of the MO^+ complexes have negative values of overlap population, with respect to the reference bonds.

Let us turn our attention to the C−H bond being cleaved in TS1. How can we understand qualitatively the weakening of the C−H bond that strongly depends on metals or the number of d electrons? This bond weakening is a direct consequence of the orbital interactions that push some C−H bonding levels up or down the highest occupied level. If C−H bonding orbitals are unoccupied, the corresponding C−H bond strength should be effectively decreased. The MOOP diagram for ScO^+, shown at the left in Figure 5, tells us that the two bonding levels with respect to the C−H bond are still fully occupied after the orbital interactions. Therefore the orbital interactions in the ScO^+/CH_4 system are not effectively working for the activation of the C−H bond. On the other hand, in the FeO^+/CH_4 and CuO^+/CH_4 systems some C−H bonding levels are pushed up and unoccupied accordingly as a result of the orbital interactions. Let us look at the MOOP diagram for CuO^+ shown at the right in Figure 5b. The C−H bonding level at −12 eV is half-occupied and another C−H bonding level at −9 eV is vacant in the triplet state although the occupancy is dependent on spin states, and therefore the C−H bond is effectively weakened and cleaved by CuO^+. A similar situation is also found in the MOOP diagram for FeO^+. Thus, the number of d electrons and the energy of the d-block orbitals are two dominant factors for the C−H bond activation by the MO^+ complexes. This is the reason that the reactivity of the late MO^+ complexes is higher than that of the early MO^+ complexes. In this way, our qualitative orbital interaction analyses reasonably explain the DFT computational results presented earlier in this paper.

Summary and Conclusions

We have computed and analyzed the reactions of the first-row MO^+ complexes (M = Sc, Ti, V, Cr, Mn, Fe, Co, Ni, and Cu) and methane, which can competitively form methanol and methyl radical. Both high-spin and low-spin potential energy surfaces were characterized in detail at the B3LYP/6-311G** level of theory. The energy diagrams toward the product methanol are uphill for the early MO^+ complexes (ScO^+, TiO^+, and VO^+); thus, these complexes are not good mediators for the formation of methanol. On the other hand, we reasonably conclude from the general profiles of the energy diagrams that the late MO^+ complexes (FeO^+, NiO^+, and CuO^+) are able to efficiently convert methane to methanol. Our DFT calculations are fully consistent with the experimental observations for the reaction efficiencies and the methanol branching ratios for MnO^+, FeO^+, CoO^+, and NiO^+. The experimental results under ICR conditions can be reasonably explained on the basis of the computed energetics of the high-spin and the low-spin energy diagrams. Since the methane hydroxylation by the CuO^+ complex is highly exothermic (−50.0 kcal/mol), we expect that CuO^+ should be a very good mediator for the production of methanol. The various reactivities of the bare MO^+ complexes would have considerable relevance to the direct hydrocarbon hydroxylations catalyzed by organometallic active centers involved in catalysts and enzymes, and our theoretical analyses will give useful insight into the reaction mechanism. Our calculations suggested that in most cases the high-spin and the low-spin potential energy diagrams have crossing points, in the vicinity of which spin inversion can take place. This nonadiabatic electronic process can play an important role in the energetics of the reaction pathway because it can lower the activation energies of TS1 and TS2. There is a crossing point prior to TS2 on the energy diagrams for the ScO^+, TiO^+, and VO^+ complexes. In sharp contrast, there are two crossing points in the entrance channel and the exit channel on the energy diagrams for the FeO^+, CoO^+, and NiO^+ complexes, which is good for the catalytic function in that the initial spin state is conserved in a single catalytic cycle. Thus, the search of spin−orbit coupling along the reaction coordinate is important for our deeper understanding of the direct methane−methanol conversion.[43]

Acknowledgment. K.Y. would like to thank a Grant-in-Aid for Scientific Research on the Priority Area "Molecular Physical Chemistry" from the Ministry of Education, Science, Sports and Culture of Japan in support of this work. Y.S. is grateful to the JSPS for a graduate fellowship. Computations were in part carried out at the Supercomputer Laboratory of Kyoto University and at the Computer Center of the Institute for Molecular Science.

JA0017965

(43) Shiota, Y.; Yoshizawa, K. To be submitted for publication.